Organic Electronics 14 (2013) 2360–2368

Contents lists available at SciVerse ScienceDirect

Organic Electronics

journal homepage: www.elsevier.com/locate/orgel

A plasmonically enhanced polymer solar cell with gold–silica core–shell nanorods

Xiaoyan Xu [a], Aung Ko Ko Kyaw [b], Bo Peng [c], Dewei Zhao [a,1], Terence K.S. Wong [a,*], Qihua Xiong [a,c,*], Xiao Wei Sun [a,*], Alan J. Heeger [b]

[a] School of Electrical and Electronic Engineering, Nanyang Technological University, Singapore 639798, Singapore
[b] Center for Polymers and Organic Solids, University of California at Santa Barbara, Santa Barbara, CA 93106, USA
[c] School of Physical and Mathematical Sciences, Nanyang Technological University, Singapore 639798, Singapore

ARTICLE INFO

Article history:
Received 23 October 2012
Received in revised form 28 March 2013
Accepted 26 May 2013
Available online 7 June 2013

Keywords:
Polymer solar cells
Au nanorods
Metallic nanoparticles
Plasmonic effects

ABSTRACT

We report the use of chemically synthesized gold (Au)–silica core–shell nanorods with the length of 92.5 ± 8.0 nm and diameter of 34.3 ± 4.0 nm for the efficiency enhancement of bulk heterojunction (BHJ) polymer solar cells. Silica coated Au nanorods were randomly blended into the BHJ layers of these solar cells. This architecture inhibits the carrier recombination at the metal/polymer interface and effectively exploits light absorption at the surface plasmon resonance wavelengths of the Au–silica nanorods. To match the two plasmon resonant peaks of the Au–silica nanorods, we employed a low bandgap polymer, poly[2,6-(4,4-bis-(2-ethylhexyl)-*4H*-cyclopenta[2,1-b;3,4-b′] dithiophene)-*alt*-4,7-(2,1,3-benzothiadiazole)] (PCPDTBT) to construct a solar cell. The absorption spectrum of PCPDTBT:[6,6]-phenyl-C_{71}-butyric acid methyl ester ($PC_{70}BM$) is relatively wide and matches the two plasmon resonance peaks of Au–silica nanorods, which leads to greater plasmonic effects. We also constructed the poly(3-hexylthiophene):[6,6]-phenyl-C_{61}-butyric acid methyl ester (P3HT:$PC_{60}BM$) cells for comparison. The absorption spectrum of P3HT:$PC_{60}BM$ only overlaps one of the plasmon resonance peak of Au–silica nanorods. The efficiency of the P3HT:$PC_{60}BM$ device incorporating optimized Au–silica nanorods is enhanced by 12.9% from 3.17% to 3.58%, which is due to the enhanced light absorption. Compared with the P3HT:$PC_{60}BM$ device with Au–silica nanorods, the PCPDTBT:$PC_{70}BM$ device with 1 wt% Au–silica nanorods concentration has a higher efficiency of 4.4% with an increase of 26%.
© 2013 Elsevier B.V. All rights reserved.

1. Introduction

Polymer solar cells (PSCs) are a promising alternative to conventional silicon solar cells due to the low-cost materials, mechanical flexibility and solution processability at low temperature [1–6]. At present, the bulk heterojunction (BHJ) architecture based on blend of semiconducting polymer (donor) and soluble fullerene derivative (acceptor), which greatly increases the interfacial area for efficient exciton dissociation, gives a reasonably high efficiency [7–12]. However, the active layer of such devices typically has to be very thin due to low carrier mobility and short exciton diffusion length of the organic semiconductor materials (5–20 nm) [13]. The optimum active layer thickness is limited to the range of 50–100 nm [13], which leads to poor light absorption. Therefore, a variety of light-trapping techniques are necessary for improving the light absorption efficiency and effective optical path length, such as new surface micro or nanostructuring techniques [14], optimization of the electromagnetic field [15] and realization of photonic crystals by bulk structuring [16].

* Corresponding authors. Address: School of Electrical and Electronic Engineering, Nanyang Technological University, Singapore 639798, Singapore. Tel.: +65 67905367; fax: +65 67933318 (Q. Xiong).
E-mail addresses: ekswong@ntu.edu.sg (T.K.S. Wong), qihua@ntu.edu.sg (Q. Xiong), EXWSun@ntu.edu.sg (X.W. Sun).
[1] Present address: Department of Electrical Engineering and Computer Science, The University of Michigan Ann Arbor, MI 48109, USA.

1566-1199/$ - see front matter © 2013 Elsevier B.V. All rights reserved.
http://dx.doi.org/10.1016/j.orgel.2013.05.038

It is necessary to increase the light absorption by the BHJ film without increasing the film thickness. Recently, metallic nanostructures that support surface plasmons have been intensively investigated due to the light scattering and localized surface plasmon resonance (LSPR) effects [17–20]. Excited surface plasmons enhance the local electric field intensity distribution around the nanostructures, which leads to the light absorption enhancement in the active layer [21]. The LSPR is excited when the frequency of the incident light matches the LSPR peak of metallic nanoparticles (NPs). The surface plasmon resonance frequency depends strongly on the size, shape, type of metal and the dielectric environment of metallic NPs [21–27]. In addition, for large metallic NPs (~100 nm) within the BHJ layer, the incident photons can be scattered strongly by metallic nanostructures into a longer propagation path in the active layer. Recently, both theoretical and experimental studies on plasmonic effects in organic and inorganic photovoltaic devices have shown interesting results [9,28,29]. Theoretically, broadband optical absorption enhancement from the LSPR effect had been verified by simulation with three dimensional finite-difference time-domain method [17]. Blending metallic NPs into the active layer could lead to multiple light scattering effect within the BHJ layer and reduce the cell resistance. However, rapid recombination of the photo-generated charge carriers will occur at the surface of bare metallic NPs because of a high surface recombination velocity [24]. In order to avoid this issue, most experimental studies embedded bare metallic NPs in the poly(3,4-ethylene-dioxythiophene): poly(styrenesulphonate) (PEDOT:PSS) soluble conducting polymer or positioned them at the interface of the indium tin oxide (ITO) coated glass substrates [9,28,30,31]. So far, the investigation on PSCs with metallic NPs blended into the BHJ layer has been limited [32–34]. Recently, gold (Au) NPs coated by a thin shell of silica were introduced into dye-sensitized solar cells (DSSC) [35]. The silica shell can efficiently prevent charge recombination and realize multiple light reflections in the active layer of DSSC. In addition, most existing studies on metallic nanostructures for plasmonic enhancement effects are focused on spherical NPs with a diameter of less than 50 nm [18].

In this work, we investigate the effect of Au–silica core–shell nanorods on PSCs based on the blend of poly(3-hexylthiophene):[6,6]-phenyl-C_{61}-butyric acid methyl ester (P3HT:PC_{60}BM) and the blend of poly[2,6-(4,4-bis-(2-ethylhexyl)-*4H*-cyclopenta[2,1-b;3,4-b] dithiophene)-*alt*-4,7-(2,1,3-benzothiadiazole)]:[6,6]-phenyl-C_{71}-butyric acid methyl ester (PCPDTBT:PC_{70}BM). The Au–silica nanorods were blended directly into a BHJ solution with different concentration. We demonstrate that Au–silica nanorods have a stronger influence on PSCs based on low bandgap polymer PCPDTBT than PSCs based on P3HT.

2. Experimental

2.1. Synthesis of Au–silica core–shell nanorods

Au nanorods were synthesized by a seed-mediated method [36]. First, the Au seed solution was prepared by borohydride reduction of 0.25 mM $HAuCl_4$ in an aqueous hexadecyltrimethylammonium bromide (CTAB) solution (10 mL, 0.1 M). For the synthesis of the Au nanorods, 10 μL of seed solution was added to an aqueous solution of $HAuCl_4$ (0.01 M, 2 mL), $AgNO_3$ (0.01 M, 0.4 mL), CTAB (0.1 M, 40 mL), ascorbic acid (0.1 M, 0.32 mL) and HCl (1.0 M, 0.8 mL). After mixing by gentle inversion for 10 s, the reaction solution was left undisturbed for 16 h. The Au nanorods were obtained by centrifugation and re-dispersed in 26.7 mL of deionized water.

Au–silica core–shell nanorods were synthesized according to a previously published procedure [37]. NaOH solution (0.1 M) was added to 2 mL of Au nanorods solution until the pH value was adjusted to 10–11. A 20 vol% solution of tetraethyl orthosilicate (TEOS) in methanol was then added (60 μL for Au nanorods). After stirring for 12 h, Au–silica core–shell nanorods were obtained by centrifugation, and re-dispersed in 3 mL ethanol. Finally, 50 μL of hexadecyltrimethoxysilane was added to obtain the core–shell solution. After stirring for 18 h at 60 °C, the hydrophobic core–shell nanostructures were obtained by centrifugation and re-dispersed in chlorobenzene (CB) or 1, 2-dichlorobenzene (DCB). The reason for dispersing the Au–silica nanorods in two separate solvents is to avoid possible co-solvent effects during fabrication of the PSC devices.

2.2. Device fabrication

The device structures are ITO/PEDOT:PSS/P3HT:PC_{60}BM/Ca/Al and ITO/PEDOT:PSS/PCPDTBT:PC_{70}BM/Ca/Al (Fig. 1). ITO coated glass substrates with a sheet resistance of 15 Ω/□ were cleaned for 15 min respectively in detergent, de-ionized water, acetone and isopropyl alcohol using an ultrasonic bath and blown dry using nitrogen. The substrate was then treated with an oxygen plasma for 3 min. PEDOT:PSS (Baytron P 4083) was spin coated at 3000 rpm for 60 s onto the ITO electrode with a thickness of ~40 nm. The ITO coated glass substrate with the PEDOT:PSS layer was then preheated on a hotplate at 150 °C for 20 min in air. A 40 mg blend of P3HT (Rieke Metals, Inc.) and PC_{60}BM (American Dye Sources, Inc.) with a weight ratio of 1:0.8 was dissolved in 1 mL of DCB to achieve a concentration of 40 mg/mL. For the P3HT:PC_{60}BM device with Au–silica nanorods, the Au–silica nanorods dispersed in DCB was diluted by adding DCB to give a 1 mL

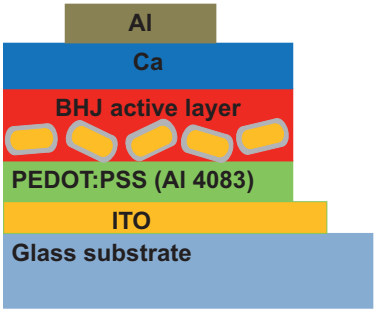

Fig. 1. Schematic of polymer solar cell with Au–silica nanorods in BHJ layer.

dispersion with a Au–silica nanorod concentration of 0.4 mg/mL. A 40 mg blend of P3HT and $PC_{60}BM$ with a weight ratio of 1:0.8 was similarly added to this DCB solution to give a P3HT:$PC_{60}BM$ blend with 1 wt% concentration of Au–silica nanorods. The reference device of P3HT:$PC_{60}BM$ and the device with Au–silica nanorods was spin coated at 500 rpm for the first 18 s and 1000 rpm for the next 10s onto the PEDOT:PSS layer. The layer thickness of P3HT:$PC_{60}BM$ and P3HT:$PC_{60}BM$ blended with 1 wt% of Au–silica nanorods were measured by profilometry to be 101 nm and 102 nm respectively. The P3HT:$PC_{60}BM$ film was dried naturally and then annealed at 140°C for 10 min. inside a glove box filled with N_2 (H_2O < 0.1 ppm and O_2 <0.1 ppm).

In a similar manner, the blend of PCPDTBT (average molecular weight 30,000 g/mol; polydispersity 2.2, 1-material, Inc.) and $PC_{70}BM$ (Ossila, Inc.) with a weight ratio of 1:3 was prepared by adding 40 mg of this blend to a mixture of 1 mL of CB and 10 mg of the processing additive 1,8 octanedithiol to facilitate phase separation. For the PCPDTBT: $PC_{70}BM$ device with Au–silica nanorods, 10 mg of 1,8 octanedithiol was added to a 1 mL CB solution containing different amounts of Au–silica nanorods. This ensures that the concentration of the processing additive is the same for both the reference device and the devices with Au–silica nanorods. A 40 mg blend of PCPDTBT and $PC_{70}BM$ with a weight ratio of 1:3 was then added to the CB solution containing 1,8 octanedithiol to yield 0.5 wt%, 1 wt% and 2 wt% of Au–silica nanorods in PCPDTBT:$PC_{70}BM$. The spin coating conditions of the reference PCPDTBT:$PC_{70}BM$ device and devices with Au–silica nanorods were adjusted to 3000 rpm for 50s so that the thickness of the BHJ layers as determined from surface profilometry were 110 nm and 112 nm respectively. Finally, a Ca (13 nm)/Al (200 nm) bilayer top electrode was subsequently vacuum-deposited at a pressure of 1×10^{-4} Pa onto the active layer. All devices had an active area of 3×3 mm^2.

2.3. Device characterization

The current–voltage (I–V) measurement was conducted with a Keithley 2400 source meter under simulated 100 mW/cm^2 (AM 1.5G) irradiation from a solar simulator (Solar Light Co. Inc.). The simulated light intensity was calibrated with a standard silicon photovoltaic cell. The incident photon to current conversion efficiency (IPCE) measurement system (Bentham PVE300) comprised of a Xenon lamp, a monochromator, a chopper, a lock-in amplifier and a calibrated silicon photodetector. The film thickness was measured by a KLA-Tencor P-10 surface profiler equipped with a stylus running on the sample surface. In addition, scanning electron microscope (SEM) cross section of the polymer blend film was imaged by a JEOL 7001F field emission (FE) SEM at an accelerating voltage of 5.0 kV. For cross sectional SEM, the polymer blend film was spin coated onto a silicon wafer to avoid sample charging. The surface roughness of the BHJ films was characterized by a tapping mode atomic force microscope (AFM) (MFP-3D, Ayslum Research). The transmission electron microscope (TEM) image of the Au–silica nanorods was acquired using a JEOL 1400 TEM with an accelerating voltage of 100 kV.

Optical absorption measurement of the polymer/fullerene films on glass was performed using a UV–visible–near IR scanning spectrophotometer (Perkin–Elmer Lamda 950) equipped with a 150 mm diameter integrating sphere. The absorption spectra were obtained by using the relation: $absorption = 100\% - T - R$, where T (%) is the total transmission and R (%) is the total reflection. In a total transmission measurement, the sample was mounted at the transmittance port of the integrating sphere and the sample reflectance port opposite was covered by a white diffuse reflector. This ensures that all light that passed through the sample was collected. For the total reflection measurement, the sample was mounted at the reflectance port with the sample normal titled at 8° with respect to the incident beam direction. The specular exclusion port was covered by a white diffuse reflector. In addition, diffuse (off-specular) transmission and reflection measurements were performed in order to obtain the haze factor. For diffuse transmission and diffuse reflection measurements, the sample reflectance and specular exclusion ports were left respectively open. The steady state photoluminescence (PL) spectra of the P3HT film and PCPDTBT solution were recorded in air under ambient conditions by a RF-5301PC fluorescence spectrometer. A 150 W Xenon lamp (530 nm and 720 nm) was used as the excitation source and the photodetector had a spectral range from 300 nm to 900 nm.

3. Results and discussion

Fig. 2a (inset) shows the TEM image of the solution-processed Au–silica core–shell nanorods [36]. The length and diameter of the Au core are 92.5 ± 8.0 nm and 34.3 ± 4.0 nm respectively and the thickness of the silica shell is 17.1 nm. The extinction spectrum of the Au–silica nanorods solution in CB measured by UV–vis spectroscopy is shown in Fig. 2a. There are two extinction peaks where localized surface plamsons are excited. The major peak is located at about 720 nm and minor peak is at about 530 nm. As demonstrated by Gan's theory [38], the wavelength of the major peak is tunable through the aspect ratio of the nanorod and thus provides a greater degree of design freedom relative to the nanosphere. The major and minor surface plasmon resonance peaks originate from the longitudinal and transverse oscillations of surface electrons respectively due to the rod shape of Au–silica nanrods [38,39]. The absorption spectrum of P3HT:$PC_{60}BM$ film shown in Fig. 2b ranges from 300 to 650 nm. The maximum absorption peak at 520 nm only matches the minor surface plasmon resonance peak of Au–silica nanorods. The absorption spectrum of PCPDTBT:$PC_{70}BM$ film shown in Fig. 2b is broader and ranges from 300 to 800 nm with a maximum absorption peak at 780 nm. Since this matches the longitudinal surface plasmon resonance peak of Au–silica nanorods, Au–silica nanorods were mixed with PCPDTBT:$PC_{70}BM$ solution to fabricate standard PSCs.

Fig. 3a shows the plan view secondary electron SEM image of a nanorod embedded in a spin-coated PCPDTBT:PC_{70}-BM film with 1 wt% Au–silica nanorods. The shape, length and diameter of this nanorod are consistent with the TEM image in fig. 2a. Due to the short range of secondary

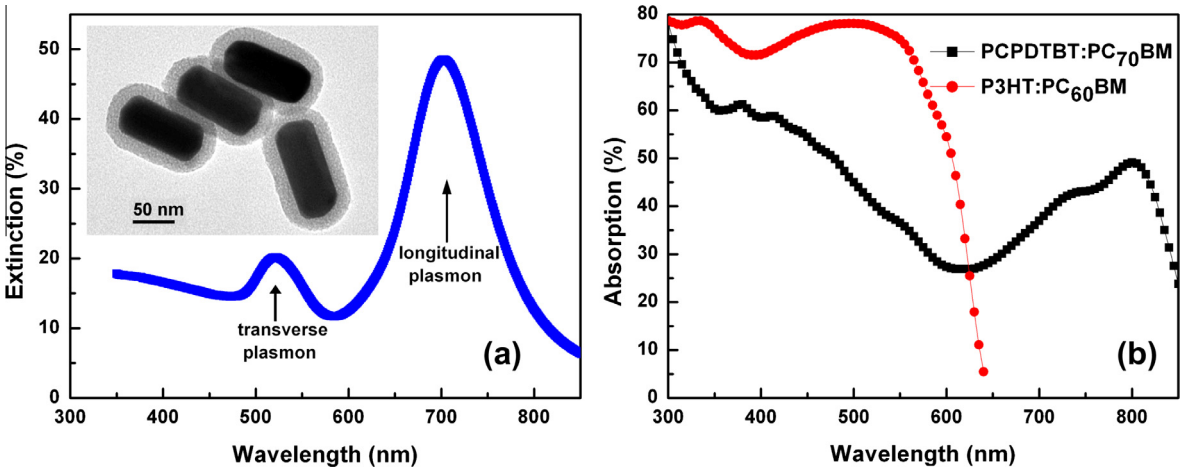

Fig. 2. Extinction spectrum of the Au–silica nanorods solution in CB with the surface plasmon resonance peaks at ~530 nm and ~720 nm. The inset is the TEM image of the Au–silica nanorods. The scale bar represents 50 nm. (b) UV/Vis absorption spectra of P3HT:$PC_{60}BM$ film (~100 nm) and PCPDTBT:$PC_{70}BM$ film (~110 nm).

electrons, this particular nanorod should be located near the surface of the PCPDTBT:$PC_{70}BM$ film with its major axis tilted with respect to the surface. In general, it is difficult to image the Au–silica nanorods using SEM as large areas of the sample surface are devoid of nanorods. Fig. 3b shows a cross section SEM image of the ~130 nm thick PCPDTBT:$PC_{70}BM$ film with a probable embedded Au–silica nanorod highlighted by the circle. The difficulty of imaging the nanorods in the film could be due to the low density of the nanorods in the sample or nanorod surface interaction with the polymer blend matrix. More convincing evidence for the incorporation of Au–silica nanorods can be seen in

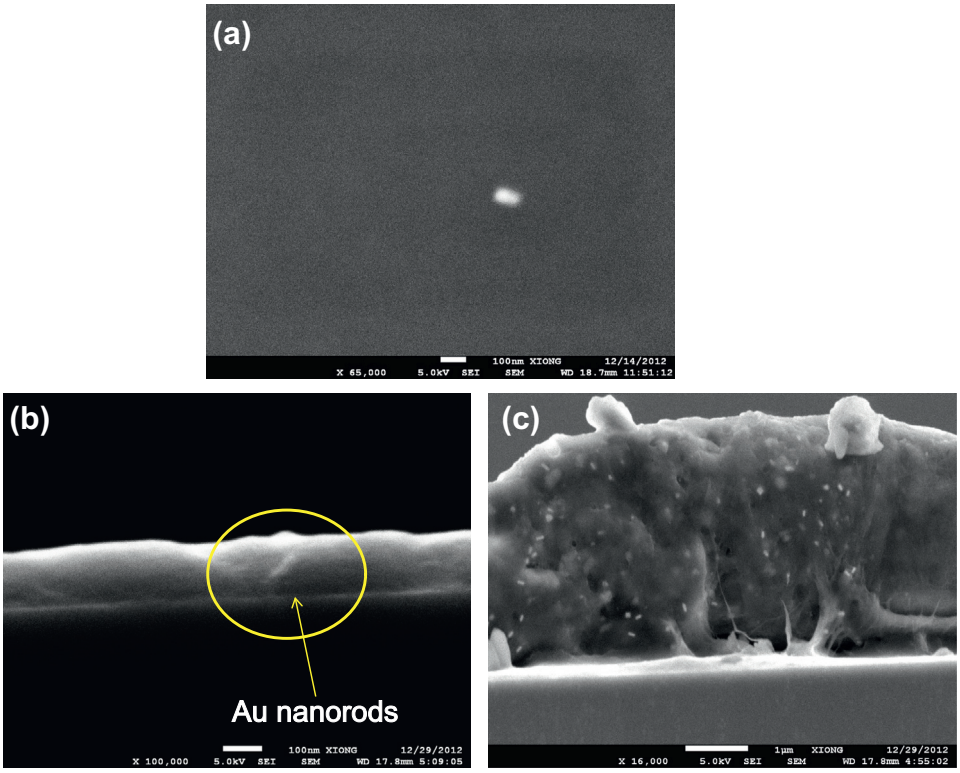

Fig. 3. (a) Plan view SEM image of a PCPDTBT:$PC_{70}BM$ film with 1 wt% Au–silica nanorod showing a nanorod near the surface; (b) cross sectional SEM image of a PCPDTBT:$PC_{70}BM$:Au–silica nanorods film; (c) cross sectional SEM image of the same film with section made near the periphery of the spin coated film. The white scale bars in (a), (b) and (c) represent 100 nm, 100 nm and 1 μm respectively.

Fig. 3c. In this image, the cross section was made near the periphery of the sample where the polymer blend layer is thicker (~3 μm). Here, the nanorods incorporated in the locally thick film can be clearly seen in random order and orientation. The SEM results are consistent with AFM topographic images. Fig. 4a–c shows the surface morphology scans of PCPDTBT:$PC_{70}BM$ films with 0 wt%, 1 wt% and 2 wt% of Au–silica nanorods respectively. The nanorods are not apparent on the surface and the root mean square (RMS) surface roughness for fig. 4a–c are 1.13 nm, 0.934 nm and 1.147 nm respectively.

For comparison, devices with BHJ layers consisting of Au–silica nanorods and P3HT:$PC_{60}BM$ were also fabricated. Fig. 5a shows the current density–voltage (J–V) characteristics of PSCs with and without Au–silica nanorods in P3HT:$PC_{60}BM$ blend under 100 mW/cm^2 illumination. For the optimized device without Au–silica nanorods, the open-circuit voltage (V_{oc}), the short-circuit current density (J_{sc}), the fill factor (FF) and the power conversion efficiency (η) are 0.622 V, 7.97 mA/cm^2, 64% and 3.17% respectively. For the device with optimized Au–silica nanorods concentration of 1 wt%, the V_{oc} remains unchanged. The J_{sc}, FF and η increase to 8.73 mA/cm^2, 66% and 3.58% respectively. As a result, the overall efficiency enhancement induced by Au–silica nanorods in PSCs based on P3HT:$PC_{60}BM$ blend is 12.9%. This improvement in efficiency was repeatable.

IPCE measurements of the reference P3HT:$PC_{60}BM$ device and the device with 1 wt% of Au–silica nanorods were conducted to better understand the origin of the improved J_{sc}. Fig. 5b shows that the IPCE spectrum of the P3HT:PC_{60}BM device with 1 wt% of Au–silica nanorods is increased with respect to the reference device spectrum within the wavelength range from 480 nm to 600 nm. Outside this range, the two spectra are essentially overlapping. The wavelength range 480–600 nm coincides with the transverse surface plasmon resonance peak of the Au–silica nanorods. Since both devices have similar absorber thickness, fig. 5b shows that the improvement in photocurrent is due to the incorporation of Au–silica nanorods. Fig. 5c presents the PL emission spectrum of a spin-coated P3HT film and a P3HT film with 1 wt% Au–silica nanorods. The

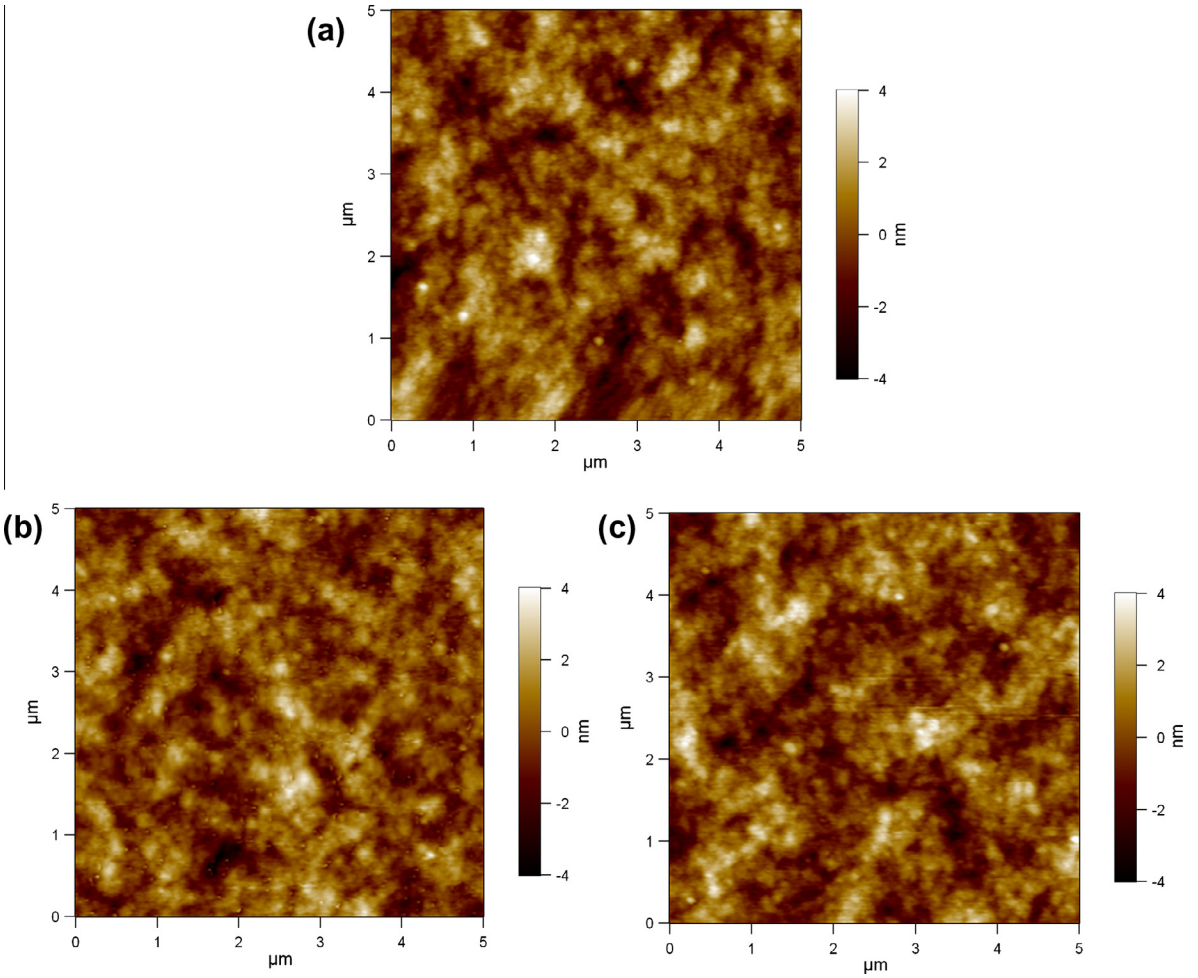

Fig. 4. AFM images of the PCPDTBT:$PC_{70}BM$ film: (a) height image of the film without Au–silica nanorods, RMS roughness = 1.130 nm; (b) height image of the film with 1 wt% Au–silica nanorods concentration, RMS roughness = 0.934 nm; (c) height image of the film with 2 wt% Au–silica nanorods concentration, RMS roughness = 1.147 nm.

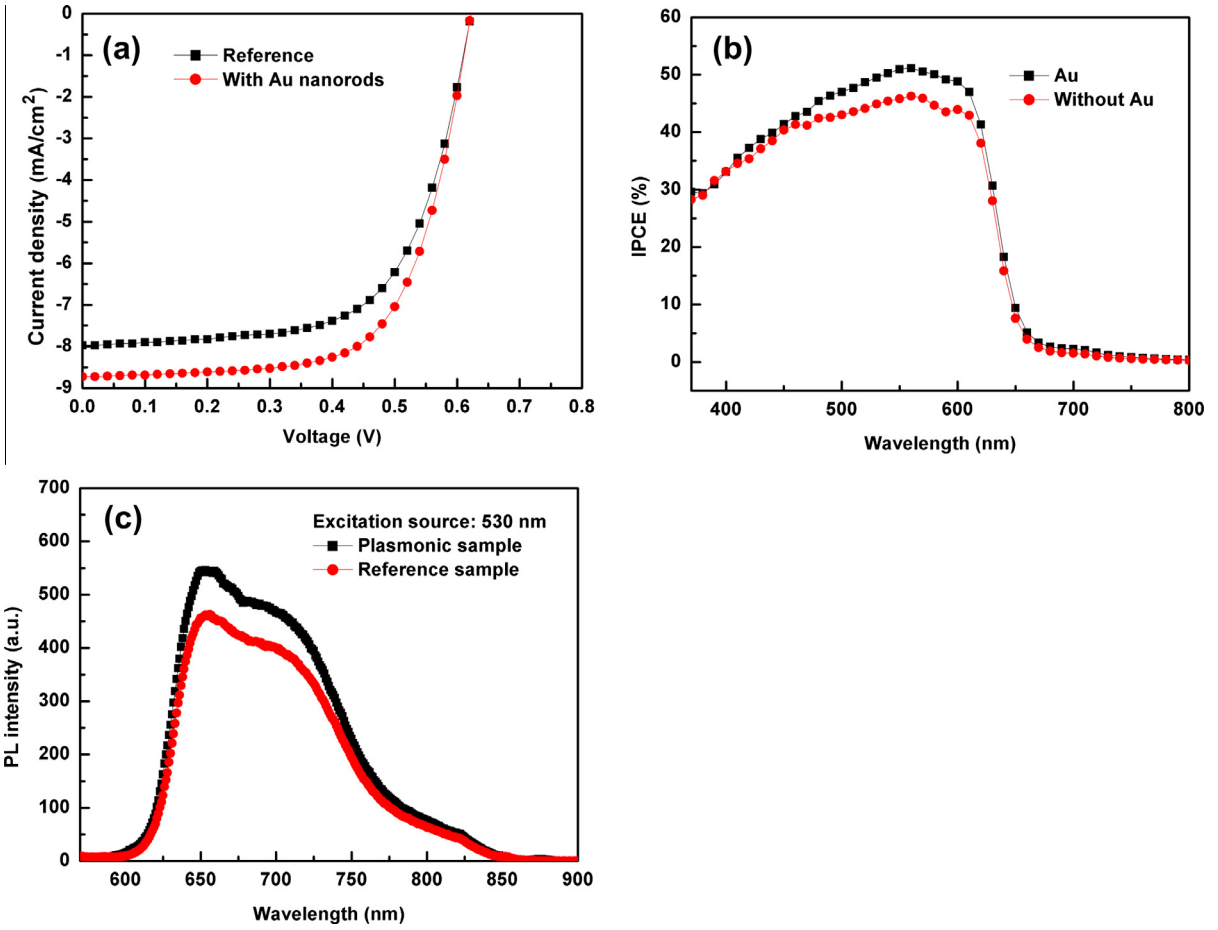

Fig. 5. (a) *J–V* characteristics of plain P3HT:$PC_{60}BM$ device and plasmonic device with 1 wt% Au–silica nanorods concentration; (b) IPCE spectra of plain P3HT:$PC_{60}BM$ devices and plasmonic device with 1 wt% Au–silica nanorods concentration; (c) PL spectra of plain P3HT:$PC_{60}BM$ film and P3HT:$PC_{60}BM$ film with 1 wt% Au–silica nanorods concentration using an excitation source wavelength of 530 nm.

excitation wavelength used for both spectra was 530 nm. The PL emission peak at 650 nm for the P3HT film with nanorods is enhanced with respect to the P3HT film. Since the excitation wavelength corresponds to the transverse surface plasmon resonance peak of the nanorods, these nanoparticles can cause an increase in the density of photogenerated excitons in the P3HT, thereby increasing the PL intensity.

Fig. 6a presents the *J–V* characteristics of PSCs with and without Au–silica nanorods in the PCPDTBT:$PC_{70}BM$ blend. For the device without Au–silica nanorods, V_{oc}, J_{sc}, *FF* and η are 0.597 V, 11.4 mA/cm^2, 51.4% and 3.50%, respectively (Table 1). For the device with 1 wt% Au–silica nanorods concentration, the V_{oc} is 0.597 V which is the same as the reference device. The J_{sc}, *FF* and η increase to 12.7 mA/cm^2, 58.1%, and 4.4%, respectively. The *FF* has the largest enhancement by 14% at this concentration and the series resistance reduced from 2.75 Ω cm^2 to 1.32 Ω cm^2 (Table 1). When the Au–silica nanorods concentration increases to 2 wt%, the *FF* decreases from 58.1% to 46.7% due to increase in both series resistance and shunt conductance. The J_{sc} does not show any further increase. Fig. 6b presents the IPCE spectra for the reference PCPDTBT:$PC_{70}BM$ device and devices incorporated with different Au–silica nanorod concentrations. The IPCE spectra of the devices with Au–silica nanorods are increased relative to the reference device spectrum over a broad wavelength range from about 500 to 800 nm. The largest increase is seen for the device with 1 wt% of nanorods. Outside this range, the spectra are overlapping. The spectral region of enhanced IPCE is in good agreement with the transverse and longitudinal surface plasmon resonance peaks of the Au–silica nanorods. Since these devices have similar absorber thickness, the Au–silica nanorods should account for the improvement in the photocurrent.

The PL spectra of PCPDTBT and PCPDTBT with 0.1 mg/mL of Au–silica nanorods dissolved in CB are shown in Fig. 6c. For the low bandgap polymer PCPDTBT, solution PL had to be performed instead of film PL because the spectral range of the detector in the PL system is limited to 300–900 nm. The PL spectrum of the PCPDTBT solution in Fig. 6c agrees with that in [40]. Fig. 6c shows that the PL intensity of the PCPDTBT solution with Au–silica nanorods is enhanced with respect to the reference PCPDTBT

Table 1
Device performance parameters of PSCs based on PCPDTBT:$PC_{70}BM$ with different Au–silica nanorod concentration under 100 mW/cm^2 AM 1.5G simulated solar irradiation.

Au–silica nanorod concentration (wt%)	V_{oc} (V)	J_{sc} (mA/cm^2)	FF (%)	PCE (%)
0	0.597	11.4	51.4	3.5
0.5	0.599	12.2	56.2	4.1
1	0.597	12.7	58.1	4.4
2	0.588	12.1	46.7	3.3

solution from 825 nm to 850 nm when excited at 720 nm. This confirms that the density of photo-generated excitons is increased when Au–silica nanorods are present in the PCPDTBT solution. Fig. 6d shows that the PCPDTBT:$PC_{70}BM$ film with 1 wt% Au–silica nanorods has greater optical absorption than the plain PCPDTBT:$PC_{70}BM$ film within the spectral range from 500 nm to 800 nm. Both layers have a thickness of 110 nm. For wavelengths below 500 nm and above 830 nm, the absorption is the same. This shows that the Au–silica nanorods increase the optical absorption of the PCPDTBT:$PC_{70}BM$ film over the spectral range spanning the two surface plasmon resonance peaks.

The main mechanisms of absorption enhancement in photovoltaic devices incorporated with metallic nanoparticles are: (i) enhanced localized electric fields at the surface plasmon resonance and (ii) increased scattering of light [19,21]. The latter effect is analogous to an anti-reflection coating if the nanoparticles are located at the surface. In order to identify the main enhancement mechanism in our PSCs with embedded Au–silica nanorods, we performed additional haze factor measurement for diffuse transmission and reflection on the PCPDTBT:$PC_{70}BM$ films [41]. Fig. 7a shows the spectrum of the haze factor for transmission defined as the ratio between the diffuse transmission and the total transmission for PCPDTBT:$PC_{70}BM$ films with and without 1 wt% Au–silica nanorods. It can be seen that for the PCPDTBT:$PC_{70}BM$ film with nanorods, the haze factor for transmission ranges between 20% and 25% from 300 nm and 850 nm which is higher than that of the reference sample (8–10%). This shows that the sample with nanorods has significantly more diffuse transmission than the reference sample. The slight increase in the haze factor

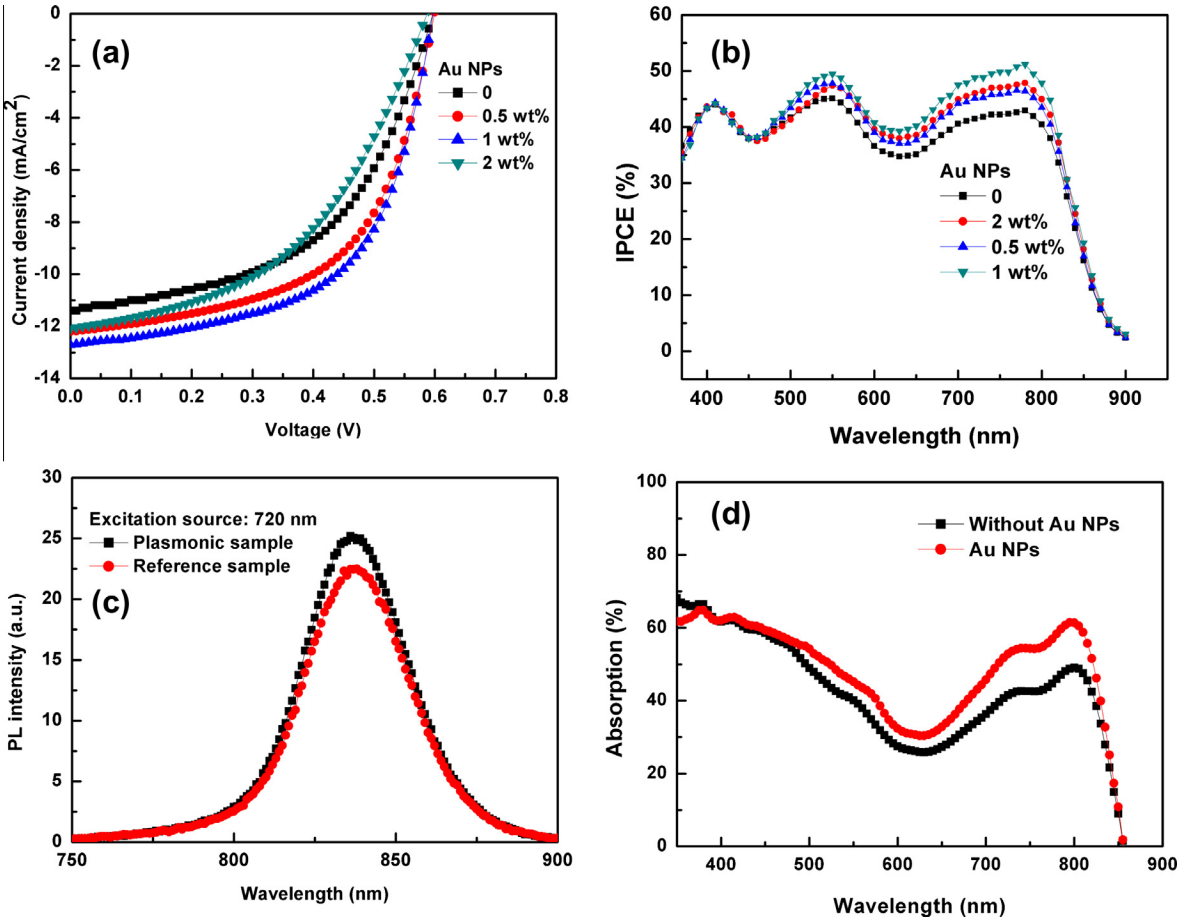

Fig. 6. (a) *J–V* characteristics of PCPDTBT:$PC_{70}BM$ devices with and without Au–silica nanorods; (b) IPCE spectra of PCPDTBT:$PC_{70}BM$ device with and without Au–silica nanorods; (c) solution PL spectra of PCPDTBT and PCPDTBT with 0.1 mg/mL Au–silica nanorods concentration in CB using an excitation source wavelengths of 720 nm; (d) UV/Vis absorption spectra of plain PCPDTBT:$PC_{70}BM$ film and BHJ film with 1 wt% Au–silica nanorods concentration. The thickness of both film layers is 110 nm.

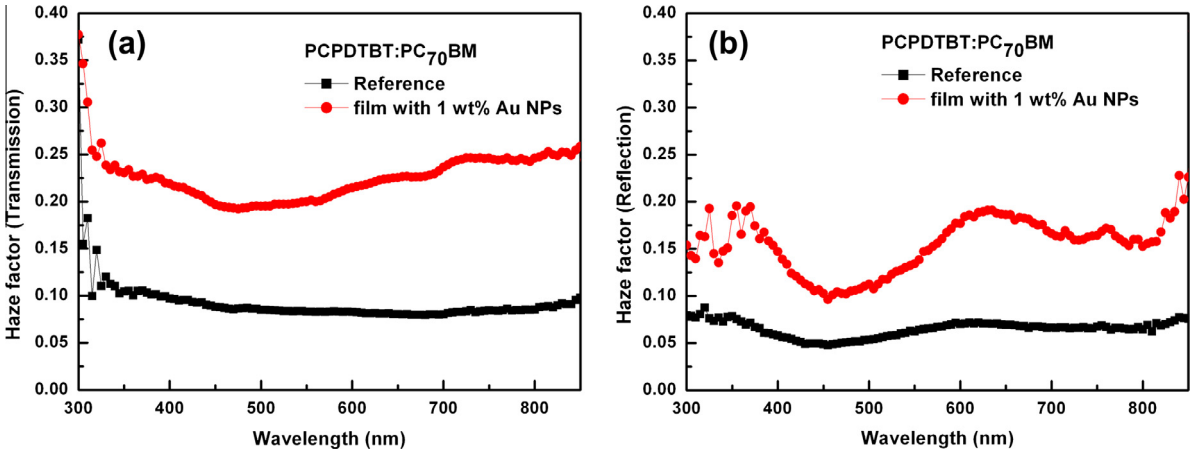

Fig. 7. (a) Transmission haze factor spectrum for PCPDTBT:$PC_{70}BM$ film with and without 1 wt% of Au–silica nanorods; (b) Reflection haze factor spectrum for PCPDTBT:$PC_{70}BM$ film with and without 1 wt% of Au–silica nanorods.

for transmission from 500 nm to 800 nm could be due to increased light scattering near the two surface plasmon resonance peaks of the Au–silica nanorods. Fig. 7b shows the spectrum of the haze factor for reflection defined as the ratio between the diffuse reflection and the total reflection for PCPDTBT:$PC_{70}BM$ films with and without 1 wt% Au–silica nanorods. For the sample with nanorods, the haze factor for reflection ranges between 10% and 20% from 300 nm to 850 nm. The corresponding range for the reference sample is 5–7.5%. Taken together, these results for the haze factor for transmission and reflection show that increased light scattering by the nanorods can account for the observed performance enhancement in the PCPDTBT:$PC_{70}BM$ devices with blended nanorods. This conclusion is consistent with the theoretical calculations of the scattering and absorption efficiencies of Au nanorods by Lee and El-Sayed [42]. For an aspect ratio (length:diameter) of 3 similar to the Au–silica nanorods used in the present work, they found that the scattering efficiency is larger than the absorption efficiency at the longitudinal plasmon resonance peak.

In the experimental study by Brown et. al. [35], spherical Au–silica nanoparticles with a shell thickness of 3–8 nm was found to increase absorption in the active layer of a DSSC by enhanced localized electric fields or resonant energy transfer. Reduction of the shell thickness of the Au–silica nanorods in this work to this range may therefore be beneficial because both light scattering and enhanced localized fields could then be effective. Further experiments are in progress to study this.

4. Conclusion

In summary, Au–silica core–shell nanorods were randomly blended into active layers of PSCs to enhance the power conversion efficiency. For PSCs based on P3HT:$PC_{60}BM$ blend, the addition of optimized Au–silica nanorods concentration of 1 wt% into BHJ layer results in efficiency enhancement of 12.9% from 3.17% to 3.58%. A low bandgap polymer system (PCPDTBT:$PC_{70}BM$) was also studied because its absorption spectrum is wide and its absorption peak matches the primary surface plasmon resonance peak of Au–silica nanorods, resulting in much stronger plasmonic effects. The device based on PCPDTBT:$PC_{70}BM$ blend with a Au–silica nanorod concentration of 1 wt% has a higher efficiency improvement (26% from 3.50% to 4.40%) than the devices based on P3HT:$PC_{60}BM$ blend with the optimized Au–silica nanorod concentration. IPCE and PL spectra confirm that incorporation of Au–silica nanorods into the BHJ film enhances light absorption at the surface plamson resonances of Au–silica nanorods. From diffuse transmission and reflection measurements, we deduced that increased light scattering by Au–silica nanorods can result in enhanced light absorption by PSCs. The enhancement is especially pronounced in the PSCs based on the low bandgap polymer PCPDTBT.

Acknowledgements

The authors gratefully acknowledge the assistance of Dr. Manohar Rao, Dr. Lam Yeng Ming and Tai Kong Fai of ERIAN, NTU for the AFM measurements. A.K.K. Kyaw thanks the Agency for Science Technology and Research (A∗STAR) of Singapore for a postdoctoral fellowship. Q.X. gratefully thanks the strong support from Singapore National Research Found through a Competitive Research Program (NRF-CRP-6-2010-2), and Singapore Ministry of Education via a Tier2 grant (MOE2011-T2-2-051).

References

[1] G. Dennler, N.S. Sariciftci, Proc. IEEE 93 (2005) 1429–1439.
[2] D. Carsten, D. Vladimir, Rep. Prog. Phys. 73 (2010) 096401.
[3] M.A. Ruderer, P. Muller-Buschbaum, Soft Matter 7 (2011) 5482–5493.
[4] C.N. Hoth, P. Schilinsky, S.A. Choulis, C.J. Brabec, Nano Lett. 8 (2008) 2806–2813.
[5] J. Jung, D. Kim, J. Lim, C. Lee, S.C. Yoon, Jpn. J. Appl. Phys. 49 (2010). 05EB031–05EB035.
[6] C.J. Brabec, Sol. Energy Mater. Sol. Cells 83 (2004) 273–292.
[7] Z. He, C. Zhong, S. Su, M. Xu, H. Wu, Y. Cao, Nat. Photon. 6 (2012) 593–597.

[8] Y.J. Cheng, C.H. Hsieh, Y. He, C.S. Hsu, Y. Li, J. Am. Chem. Soc. 132 (2010) 17381–17383.
[9] J. Yang, J. You, C.C. Chen, W.C. Hsu, H.R. Tan, X.W. Zhang, Z. Hong, Y. Yang, ACS Nano 5 (2011) 6210–6217.
[10] Y. Liang, Z. Xu, J. Xia, S.T. Tsai, Y. Wu, G. Li, C. Ray, L. Yu, Adv. Mater. 22 (2010) E135–E138.
[11] S.H. Park, A. Roy, S. Beaupré, S. Cho, N. Coates, J.S. Moon, D. Moses, M. Leclerc, K. Lee, A.J. Heeger, Nat. Photon. 3 (2009) 297–303.
[12] H.-Y. Chen, J. Hou, S. Zhang, Y. Liang, G. Yang, Y. Yang, L. Yu, Y. Wu, G. Li, Nat. Photon. 3 (2009) 649–653.
[13] S.R. Forrest, MRS Bull. 30 (2005) 28–32.
[14] R. Bouffaron, L. Escoubas, J.J. Simon, P. Torchio, F. Flory, G. Berginc, P. Masclet, Opt. Express 16 (2008) 19304–19309.
[15] F. Monestier, J.-J. Simon, P. Torchio, L. Escoubas, F. Flory, S. Bailly, R. de Bettignies, S. Guillerez, C. Defranoux, Sol. Energy Mater. Sol. Cells 91 (2007) 405–410.
[16] D. Duch, L. Escoubas, J.J. Simon, P. Torchio, W. Vervisch, F. Flory, Appl. Phys. Lett. 92 (2008) 193310.
[17] J. Zhu, M. Xue, H. Shen, Z. Wu, S. Kim, J.J. Ho, A. Hassani-Afshar, B. Zeng, K.L. Wang, Appl. Phys. Lett. 98 (2011) 151110.
[18] J.L. Wu, F.C. Chen, Y.S. Hsiao, F.C. Chien, P. Chen, C.H. Kuo, M.H. Huang, C.S. Hsu, ACS Nano 5 (2011) 959–967.
[19] K.R. Catchpole, S. Mokkapati, F. Beck, E.C. Wang, A. McKinley, A. Basch, J. Lee, MRS Bull. 36 (2011) 461–467.
[20] B. Peng, Q. Zhang, X. Liu, Y. Ji, H.V. Demir, C.H.A. Huan, T.C. Sum, Q. Xiong, ACS Nano 6 (2012) 6250–6259.
[21] H.A. Atwater, A. Polman, Nat. Mater. 9 (2010) 205–213.
[22] K.R. Catchpole, A. Polman, Opt. Express 16 (2008) (1800) 21793–21800.
[23] V.E. Ferry, J.N. Munday, H.A. Atwater, Adv. Mater. 22 (2010) 4794–4808.
[24] W.J. Yoon, K.Y. Jung, J. Liu, T. Duraisamy, R. Revur, F.L. Teixeira, S. Sengupta, P.R. Berger, Sol. Energy Mater. Sol. Cells 94 (2010) 128–132.
[25] O. Stenzel, A. Stendal, K. Voigtsberger, C. von Borczyskowski, Sol. Energy Mater. Sol. Cells 37 (1995) 337–348.
[26] A.P. Kulkarni, K.M. Noone, K. Munechika, S.R. Guyer, D.S. Ginger, Nano Lett. 10 (2010) 1501–1505.
[27] J. Pei, J. Tao, Y. Zhou, Q. Dong, Z. Liu, Z. Li, F. Chen, J. Zhang, W. Xu, W. Tian, Sol. Energy Mater. Sol. Cells 95 (2011) 3281–3286.
[28] T.H. Reilly, J. Van De Lagemaat, R.C. Tenent, A.J. Morfa, K.L. Rowlen, Appl. Phys. Lett. 92 (2008) 243304.
[29] S. Pillai, K.R. Catchpole, T. Trupke, M.A. Green, J. Appl. Phys. 101 (2007) 093105.
[30] A.J. Morfa, K.L. Rowlen, T.H. Reilly, M.J. Romero, J. Van De Lagemaat, Appl. Phys. Lett. 92 (2008) 013504.
[31] M. Westphalen, U. Kreibig, J. Rostalski, H. Lüth, D. Meissner, Sol. Energy Mater. Sol. Cells 61 (2000) 97–105.
[32] F.X. Xie, W.C.H. Choy, C.C.D. Wang, W.E.I. Sha, D.D.S. Fung, Appl. Phys. Lett. 99 (2011) 153304.
[33] C.C.D. Wang, W.C.H. Choy, C. Duan, D.D.S. Fung, W.E.I. Sha, F.X. Xie, F. Huang, Y. Cao, J. Mater. Chem. 22 (2012) 1206–1211.
[34] D.H. Wang, D.Y. Kim, K.W. Choi, J.H. Seo, S.H. Im, J.H. Park, O.O. Park, A.J. Heeger, Angew. Chem. Int. Ed. 50 (2011) 5519–5523.
[35] M.D. Brown, T. Suteewong, R.S.S. Kumar, V. D'Innocenzo, A. Petrozza, M.M. Lee, U. Wiesner, H.J. Snaith, Nano Lett. 11 (2011) 438–445.
[36] T. Ming, L. Zhao, Z. Yang, H. Chen, L. Sun, J. Wang, C. Yan, Nano Lett. 9 (2009) 3896–3903.
[37] I. Gorelikov, N. Matsuura, Nano Lett. 8 (2008) 369–373.
[38] R. Gans, Ann. Phys. 47 (1915) 270.
[39] S. Link, M.A. El-Sayed, J. Phys. Chem. B 103 (1999) 8410–8426.
[40] F. Chen, D. Deng, J. Mater. Sci. 24 (2013) 871–874.
[41] Y.S. Hsiao, C.P. Chen, C.H. Chao, W.T. Whang, Org. Electron. 10 (2009) 551–561.
[42] K.S. Lee, M.A. El-Sayed, J. Phys. Chem. B 109 (2005) 20331–20338.